

# Sublattice Dichotomy in Monolayer FeSe Superconductor

Cui Ding,<sup>1,2,\*</sup> Zhipeng Xu,<sup>3,4,\*</sup> Xiaotong Jiao,<sup>1</sup> Qiyin Hu,<sup>1</sup> Wenxuan Zhao,<sup>1</sup> Lexian Yang,<sup>1,5</sup>  
Kun Jiang,<sup>3,4</sup> Jin-Feng Jia,<sup>2,6,7</sup> Lili Wang,<sup>1,5</sup> Jiangping Hu,<sup>3,8</sup> and Qi-Kun Xue<sup>1,2,5,6</sup>

<sup>1</sup>State Key Laboratory of Low-Dimensional Quantum Physics,  
Department of Physics, Tsinghua University, Beijing 100084, China

<sup>2</sup>Quantum Science Center of Guangdong-HongKong-Macao Greater Bay Area, Shenzhen 518045, China

<sup>3</sup>Beijing National Laboratory for Condensed Matter Physics and Institute of Physics, Chinese Academy of Sciences, Beijing 100190, China

<sup>4</sup>School of Physical Sciences, University of Chinese Academy of Sciences, Beijing 100190, China

<sup>5</sup>Frontier Science Center for Quantum Information, Beijing 100084, China

<sup>6</sup>Department of Physics, Southern University of Science and Technology, Shenzhen 518055, China

<sup>7</sup>Department of Physics and Astronomy, Shanghai Jiao Tong University, Shanghai 200240, China

<sup>8</sup>New Cornerstone Science Laboratory, Beijing, 100190, China

(Dated: June 24, 2024)

The pairing mechanism behind the monolayer FeSe is one essential question for iron-based superconductors. In this work, we show the sublattice degree of freedoms of monolayer FeSe plays a special role in its pairing properties, namely the sublattice dichotomy. The high-quality monolayer FeSe samples with atomic flat  $1 \times 1$  topography on the SrTiO<sub>3</sub>(001) substrates are grown by MBE. By comparing the tunneling spectra at  $\alpha$  and  $\beta$  Fe sublattices, we find the coherence peak of  $\alpha$ -Fe at the inner gap  $+V_i$  is higher than  $\beta$ -Fe while the coherence peak of  $\beta$ -Fe at  $-V_i$  is higher than  $\alpha$ -Fe with a similar amount. We also observed a reversed effect at the outer gap  $\pm V_o$ . We propose the  $\eta$ -pairing mechanism between  $k$  and  $-k + Q$  is the key mechanism for this unconventional sublattice dichotomy effect.

Monolayer FeSe grown on SrTiO<sub>3</sub> (001) is one unique iron-based high-temperature superconductor, whose superconducting transition temperature  $T_c$  about 50 ~ 65K is greatly larger than its bulk value 9 K [1–7]. Since it was discovered in 2012 [1], tremendous efforts have been spent on reproducing, analyzing and generalizing this unexpected finding [8–20]. However, owing to the sample quality and limited characterization tools, the understanding of the physical properties of monolayer FeSe, especially their superconducting nature, remains controversial. For example, the monolayer FeSe only contains Fermi surfaces (FSs) around the Brillouin zone corner while the common iron superconductors have another group of  $\Gamma$  hole pockets [8–12]. Hence, whether the superconducting features deviate from other iron-based superconductors is widely debated.

On the other hand, owing to the special structure of iron-based superconductors, they have two Fe sublattices  $\alpha$ -Fe and  $\beta$ -Fe as illustrated in Fig.1(a), which provide another degree of freedom among other high-temperature superconductors. The inversion symmetry sitting at the center of the Fe-Se square (indicated in Fig.1(a)) links these two sublattices, making their identical physical properties. However, for the monolayer FeSe on SrTiO<sub>3</sub>(001), the distances between the Se<sub>+</sub>-Fe plane and the Se<sub>-</sub>-Fe plane become asymmetric due to interface coupling [21, 22]. This fact leads to two inequivalent Fe sublattices  $\alpha$  and  $\beta$ . In this work, we carry out a systematic investigation of atomically flat monolayer FeSe using high-resolution scanning tunneling microscopy/spectroscopy (STM/STS). We find the tunneling spectra of  $\alpha$ -Fe and  $\beta$ -Fe are significantly different, resulting in the sublattice dichotomy as illustrated in Fig.1(b). More specifically, monolayer FeSe is one two-band system with two superconducting gaps  $\Delta_i$  and  $\Delta_o$ . We find that the coherence peak at  $-\Delta_i$  for  $\alpha$ -

Fe is lower than  $\beta$ -Fe while the coherence peak at  $+\Delta_i$  for  $\alpha$ -Fe is higher than  $\beta$ -Fe. This unconventional behavior deeply relates to the unconventional pairing property of monolayer FeSe.

Our experiments were carried out in a Createc ultrahigh vacuum low-temperature STM system equipped with a molecular beam epitaxy (MBE) chamber. The base pressure is better than  $1.0 \times 10^{-10}$  Torr. The Nb-doped SrTiO<sub>3</sub>(001) (0.05 wt.%) substrates were annealed above 1000 °C to obtain dual-TiO<sub>2- $\delta$</sub> -termination. FeSe films were then grown by co-evaporating high-purity Fe (99.995%) and Se (99.999 %) from standard Knudsen cells at a substrate temperature of 380 °C. The K-cell temperatures of Fe and Se were 1010 °C and 85 °C, respectively, corresponding to a deposition rate of ~ 0.02 monolayer per minute. At last, the samples were annealed at ~ 450 °C for 1 hour to remove excess Se atoms. All STM measurements were performed in a constant current mode (tunneling current set point  $I_t = 500$  pA) under liquid Helium cooling (LHe, at 4.8 K), with a polycrystalline PtIr tip and the bias voltage ( $V_s$ ) applied to the sample. The differential conductance  $dI/dV$  spectra, characterizing the local density of states around the Fermi level, are measured by disabling the feedback circuit, sweeping the sample voltage  $V_s$ , and then extracting the differential tunneling current  $dI/dV$  using a standard lock-in technique with a small bias modulation (~1% of the sweeping range) at 937 Hz. The FeSe/STO films were in-situ transferred to the angle-resolved photoemission spectroscopy (AREPS) chamber and measured under an ultrahigh vacuum below  $1.5 \times 10^{-10}$  mbar. Data were collected using a DA30 analyzer and Scienta VUV 5050 helium lamp at 80 K. The energy and angular resolutions were set to 10 meV and 0.2°, respectively.

To show the sample quality, we performed the bias-

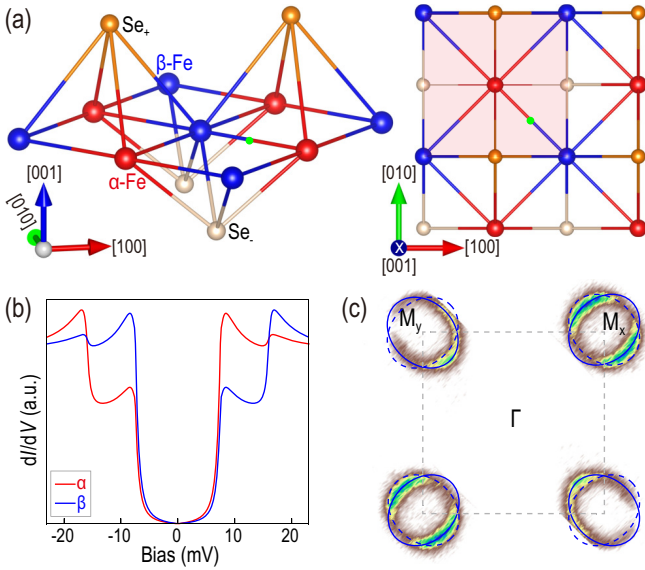


FIG. 1. (a) Schematic of the lattice of monolayer FeSe showing two inequivalent  $\alpha$ -Fe and  $\beta$ -Fe sublattices. The red and blue balls belong to  $\alpha$ -Fe and  $\beta$ -Fe respectively. The green dot indicates the position of the inversion operator for the bulk FeSe. The in-plane lattice constant  $a_0$  is equal to that of SrTiO<sub>3</sub>(001) surface  $\sim 3.89$  Å. (b) Schematic tunneling spectra in  $\alpha$ -Fe and  $\beta$ -Fe sublattices show the sublattice dichotomy. (c) The Fermi surface represented by the photoemission intensity map at the Fermi energy at 80 K. The intensity was integrated over a window ( $E_F - 25$  meV,  $E_F + 15$  meV). The map is obtained by mirroring the data around  $M_x$  and  $M_y$  with respect to the  $\Gamma$ -X direction.

dependent atomic resolution topography measurement of monolayer FeSe, as plotted in Figs. 2 (a) and (b). Fig. 2 (a) shows the atomic resolution topography of the monolayer FeSe taken at a sample bias  $V_s = 80$  mV, presenting the top layer Se(001) surface. The fast Fourier transformed (FFT) images as inserted show exclusively  $(1 \times 1)$  Bragg spots, instead of the ubiquitous  $(2 \times 1)$  orders observed in previous reports [1, 13]. The sharp  $q_a$  and  $q_b$  Bragg spots give equal in-plane lattice constants of 3.89 Å instead of the bulk FeSe 3.78 [23], which shows FeSe monolayer is fully strained to the SrTiO<sub>3</sub>(001). With the lattice of monolayer FeSe lattice superimposed, we define the sublattice Fe in the bottom-layer Se<sub>-</sub>[100]-row (top-layer Se<sub>+</sub>-[010]-row) as  $\alpha$ -Fe and another as  $\beta$ -Fe. As shown in Fig. 2(b) at  $V_s = -50$  mV, the density of states from Fe sites increases with decreasing bias. Correspondingly, the  $q_x$  and  $q_y$  Bragg spots become intense while the  $q_a$  and  $q_b$  Bragg spots remain sharp. Hence, we can identify the position of Fe-sites, as shown from the zoom-in topography measurement in Fig. 2(b) lower inset. This high-quality sample and the atomic resolution topography are the foundation for exploring the intrinsic superconducting properties of the monolayer FeSe.

After obtaining the high-quality FeSe sample, it is better to extract the electronic structure information. We perform an ARPES measurement on our sample. We integrate over

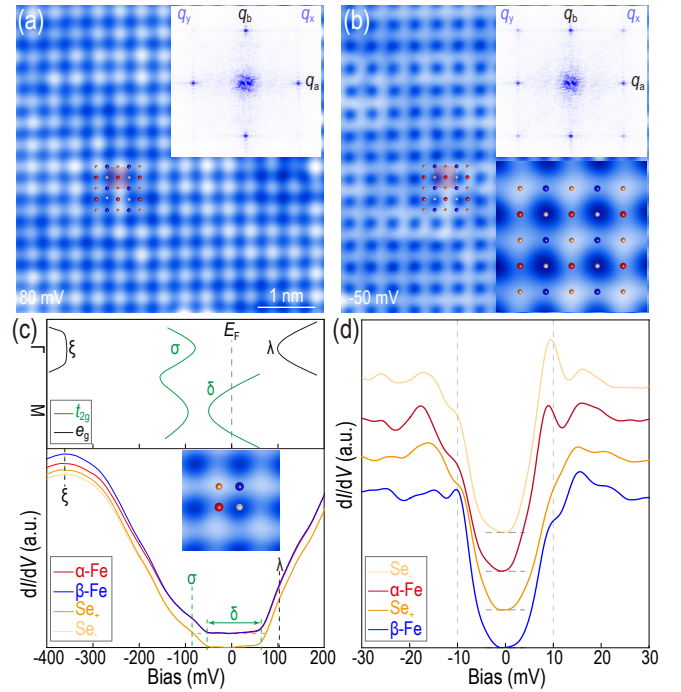


FIG. 2. (a) and (b) Bias-dependent atomic resolution topography of monolayer FeSe, with the corresponding FFT patterns inserted showing exclusive  $(1 \times 1)$  periodicity. The superimposed red and blue balls mark  $\alpha$ -Fe and  $\beta$ -Fe sites respectively, and dark and light orange balls mark upper-Se and bottom-Se sites, respectively. (c) Large-bias tunneling spectra taken at the four Fe/Se atom positions labeled in the inset, with the deduced electronic bands, in combination with ARPES results, plotted in the upper panel. The spectra are offset for clarity, with horizontal dashed lines indicating zero conductance. (d) Small-bias  $dI/dV$  tunneling spectra taken at the same positions of (c). The vertical dashed lines in (d) are eye guides for the coherence peaks  $\pm V_i$  for inner gap at  $\pm 10$  meV. Setpoint: (a)  $V_s = 80$  mV; (b)  $V_s = -50$  mV; (c)  $V_s = 500$  mV; and (d)  $V_s = 50$  mV.

the intensity in the window ( $E_F - 25$  meV,  $E_F + 15$  meV) and obtain the Fermi surfaces (FSs) in Fig. 1(c). There are two overlapping FSs around the Brillouin zone (BZ) corner while the  $\Gamma$  hole pocket is missing. This observation is consistent with previous work [8–12]. Additionally, we link the tunneling spectrums with electronic structures in Fig. 2(c). The top panel illustrates the electronic dispersions around  $E_F$  and the bottom panel summarizes the typical large-bias tunneling spectra taken at the four Fe/Se atom positions labeled in the inset. The  $dI/dV$  spectra show relatively low tunneling conductance around  $E_F$  ranging from  $-50$  meV to  $60$  meV (inferred as  $\delta$ ). The spectra upturn around  $-90$  meV belongs to the  $\sigma$  band and the high-energy one above  $100$  meV belongs to the  $\lambda$  band. The hump below  $-300$  meV comes from the  $e_g$   $\xi$  band. Hence, our measurements agree well with the band structure disclosed by ARPES and previous reports [9–12]. Then, we can move to the small-bias spectra within the range  $\pm 30$  meV plotted in Fig. 2 (d). The tunneling spectra present the standard dual-gap structures with the inner coher-

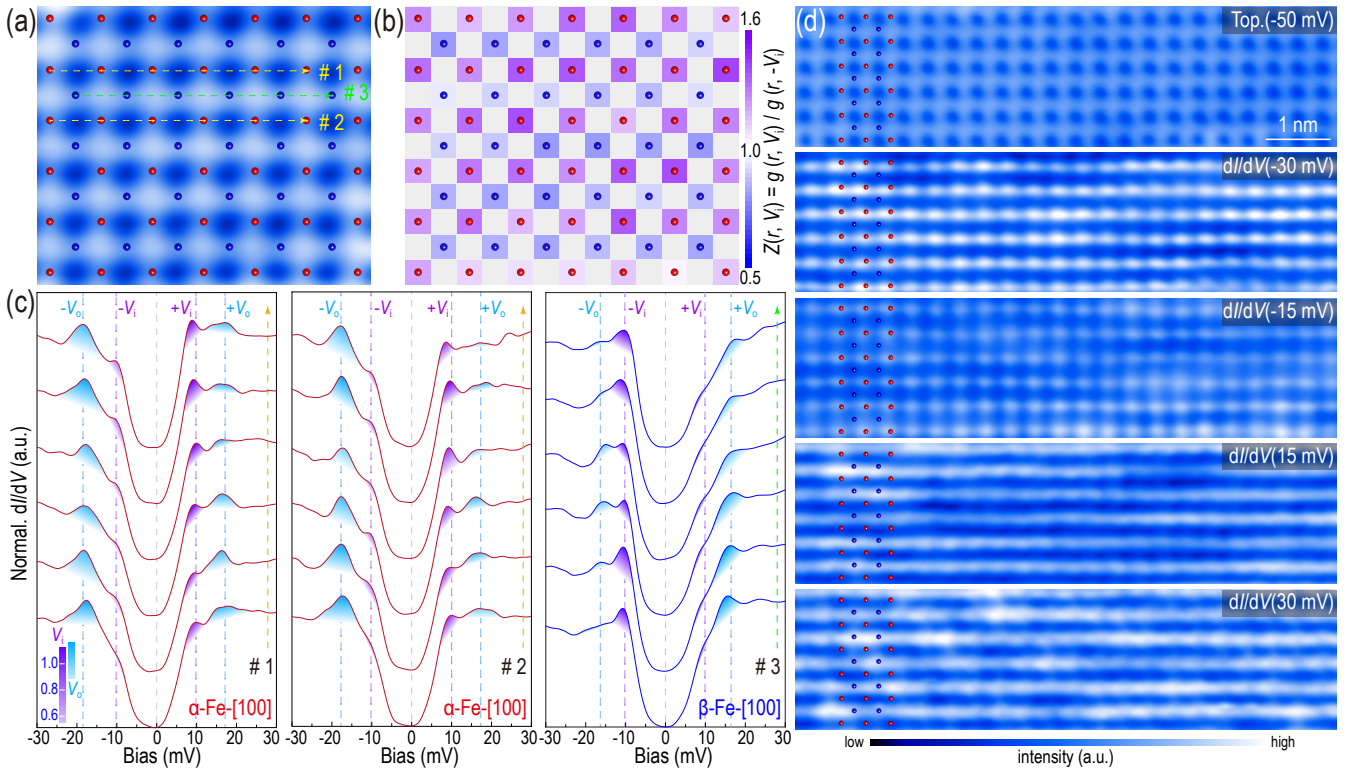


FIG. 3. (a) Atomic resolution topography of the monolayer FeSe on the SrTiO<sub>3</sub>(001) surface ( $V_s = -50$  mV), with the schematic of Fe sites overlaid. We take line cuts #1, #2 along the  $\alpha$ -Fe-[100] and the line cut #3 along  $\beta$ -Fe-[100] rows. (b) Mosaic plots of  $Z(r, V_i) = g(r, +V_i)/g(r, -V_i)$  of Fe sites as depicted in (a).  $Z(r, V_i) > 1$  for most  $\alpha$ -Fe and  $Z(r, V_i) < 1$  for most  $\beta$ -Fe. (c) Normalized tunneling spectra  $dI/dV$  ( $V_s = 50$  mV) taken along the  $\alpha$ -Fe-[100] and  $\beta$ -Fe-[100] rows highlighted in (a). (d) Topographic image ( $V_s = -50$  mV) and bias-dependent  $dI/dV$  mapping images of the same region. We can see the  $\alpha$ -Fes are more bright in -30 meV and -15 meV while the  $\beta$ -Fes are more bright in 30 meV and 15 meV. This phenomenon is inverse in (b).

ence peak  $\pm V_i$  around  $\pm 10$  meV and the outer coherence peaks  $\pm V_o$  around  $\pm 15$  meV, which are also consistent with previous works [1, 13, 14, 24]. Interestingly, all the tunneling spectra show strong particle-hole asymmetry, which can be categorized into  $\alpha$ -Fe and  $\text{Se}_-$  group and  $\beta$ -Fe and  $\text{Se}_+$  group.

Furthermore, we performed detailed low-energy tunneling measurements on each Fe atom. The normalized tunneling spectra within  $\pm 30$  meV along the three cuts marked in Fig.3(a) are plotted in Fig.3(c). We first look at the  $\alpha$ -Fe-[100] along the yellow dashed-line cut-1 (left panel in Fig.3(c)). These tunneling spectra are almost homogeneous, which further proves the high sample quality. We can see the  $\pm V_i$  coherence peaks remain constant around 10 meV while the  $\pm$

$V_o$  coherence peaks vary around  $\pm (15-17)$  meV. The outer gap variation is from the local electronic structure inhomogeneity owing to the SrTiO<sub>3</sub> substrate. On the other hand, the inner peak is closer to the Fermi energy resulting in a relatively small gap variation. One special point we need to mention here is that the tunneling spectra are obviously particle-hole asymmetric. Especially, the inner gap coherence peak is much higher on the electron side  $+V_i$ . We also take another tunneling scan of the  $\alpha$ -Fe-[100] along the yellow dashed-line cut-2, as shown in the middle panel. The spectra show similar behaviors. The electron side  $+V_i$  of the inner coherence peak is still higher than the hole side  $-V_i$ .

Then, we move to the  $\beta$ -Fe-[100]. We also obtain homogeneous tunneling spectra for  $\beta$ -Fe along the green cut-3 in the right panel. A similar two-gap feature remains for the  $\beta$ -Fe sites with the inner coherence peaks still around  $\pm V_i$  and the outer coherence peaks around  $\pm V_o$ . The gap variation for the

inner coherence peak retains small as in  $\alpha$ -Fe. Surprisingly, a new feature emerged from the asymmetric tunneling spectra at  $\pm V_i$ . For the  $\beta$ -Fe sites, the electron side  $-V_i$  of the inner coherence peaks become higher than the hole side  $+V_i$ . Hence, the tunneling spectra for the  $\alpha$ -Fe and  $\beta$ -Fe are completely



different, resulting in a sublattice dichotomy for the tunneling spectra. To further demonstrate this feature, we take a complete scan of the area in Fig.3(a) for the statistics. We define a ratio of coherence peak intensity  $Z(r, V) = g(r, V)/g(r, -V)$  at  $V = V_i$ , where  $g(r, V)$  is the normalized conductance  $dI/dV$ . The ratios  $Z(r, V_i)$  at  $V_i = 10$  meV are plotted in Fig.3(b). For the  $\alpha$ -Fe, we can see  $Z(r, V_i)$  is larger than 1 while  $Z(r, V_i) < 1$  for  $\beta$ -Fe. This particle-hole intensity switching behavior at  $\pm V_i$  is the sublattice dichotomy defined in Fig.1(b). On the other hand, the widening  $\pm V_o$  coherence peaks range within  $\pm(15-17)$  meV resulting in large errors in  $Z(r, V_o)$ . Hence, we try another strategy using  $dI/dV$  mapping at bias beyond  $V_i$  to show the sublattice dichotomy further. Fig. 3 (d) summarizes the topography and the  $g(r, V)$  mapping images at  $V_s = \pm 15$  mV and  $\pm 30$  mV. The  $\alpha$ -Fe-[100] rows consistently show a lower intensity at the hole side and a higher intensity at the electron side. Again the  $\beta$ -Fe-[100] rows consistently show the exactly reversed contrast. That is, the sublattice difference around  $\pm V_o$  maintains within (15-30) meV is exactly inverse to that at  $\pm V_i$ . Therefore, the results shown in Fig. 3 perfectly present the Fe-sublattice dichotomy illustrated in Fig. 1(b).

Let's briefly summarize what we find here. Two typical tunneling spectra  $\alpha$ -Fe and  $\beta$ -Fe are plotted in Fig.4 (a). For the inner coherence peak, the  $\beta$ -Fe has a more pronounced hole peak at  $-V_i$  while the  $\alpha$ -Fe has a more pronounced electron peak at  $+V_i$ . On the other hand, the outer coherence peak shows a reverse behavior at  $\pm V_o$ . Looking closely at Fig.4 (a), we can also find the tunneling spectra  $\alpha$ -Fe and  $\beta$ -Fe are almost dual. More precisely, the  $+V_i$  tunneling weight at  $\alpha$ -Fe is almost equal to the  $-V_i$  tunneling weight at  $\beta$ -Fe and vice versa. This unexpected phenomenon points to a highly unusual pairing function inside the monolayer FeSe. Normally, two different sublattices may behave with different gap sizes in multi-lattice superconductors. This dual effect strongly indicates a new pairing mechanism beyond conventional consideration, which reminds us of the early proposal for  $\eta$  pairing in iron-based superconductors proposed by Hu in Ref. [25].

Theoretically, it is always convenient to think from 1-Fe unit cell rather than the 2-Fe unit cell in the original lattice for the Fe-based superconductors. The BZ corresponding to 1 Fe/cell is twice as large as that of 2 Fe/cell. So we need to fold Fermi surfaces back into the smaller BZ to obtain the full Fermi surfaces, as done in Fig.4(c), which is consistent with the observed FS in Fig.1(c). In a uniform superconducting phase, the total momentum for the Cooper pairs (modulo a reciprocal lattice vector) should be zero. Normally, one focuses on the normal pairing between electrons at  $\mathbf{k}$  and  $-\mathbf{k}$  as shown in Fig.4(c). On the other hand, the momentum vector  $\mathbf{Q} = (\pi, \pi)$  in 1-Fe BZ becomes a reciprocal lattice vector for 2-Fe unit cell. Hence, besides the normal pairing order parameters connecting  $k$  and  $-k$ , the  $\eta$  pairing connecting  $k$  and  $-k + \mathbf{Q}$  is also a symmetry-allowed pairing channel, as an extension for the  $\eta$  pairing in Ref. [26, 27]. Considering the Fermi surfaces of the monolayer FeSe/SrTiO<sub>3</sub> are two electron pockets separated by  $\mathbf{Q}$ , the  $\eta$  pairing is actually inter-band pairing. The inter-band pairing is known to produce the two-gap fea-

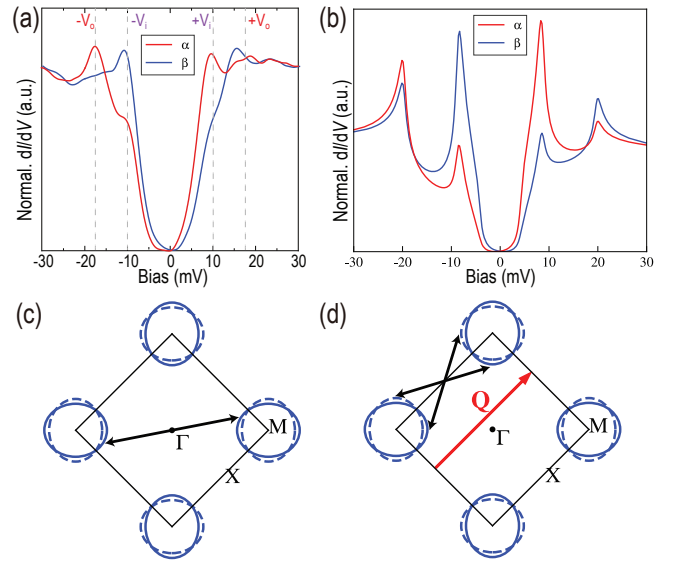


FIG. 4. (a) Two typical tunneling spectra at  $\alpha$  and  $\beta$  Fe respectively showing the sublattice dichotomy effect. (b) The calculated tunneling DOS at two sites based on the  $k \cdot p$  model with both  $\eta$  and normal pairing. (c) Fermi surface of FeSe and the systematic illustration of the normal pairing between  $k \uparrow, -k \downarrow$ . We also differentiate the two FSs in the 1-Fe unit cell by the dashed lines. (d) Systematic illustration of the  $\eta$  pairing between  $k \uparrow, -k + \mathbf{Q} \downarrow$ , where  $\mathbf{Q} = (\pi, \pi)$ .

ture and the combined action of  $\eta$  pairing and normal pairing is expected to produce the dichotomy effect [28].

In order to capture the above physics and monolayer FeSe electronic structure, we follow the  $k \cdot p$  model around  $M$  point based on the symmetry [29]. The parameters are adjusted for the normal state Hamiltonian. Then, we add both  $\eta$  pairing and normal pairing into the  $k \cdot p$  model. The local DOSs at two sublattice sites are further calculated respectively. The model details of the model are listed in the Supplemental Material. The tunneling DOSs for  $\alpha$  and  $\beta$  Fe are plotted in Fig.4(b). Obviously, the simulation including  $\eta$ -pairing confirms the sublattice dichotomy effect.

In summary, we perform a systematic investigation on the sublattice degree of freedom of the monolayer FeSe. We successfully grow the high-quality monolayer FeSe on the SrTiO<sub>3</sub>(001) substrates by MBE. Our samples show atomic-flat topography with  $1 \times 1$  Bragg spots instead of  $2 \times 1$  reconstruction. The electronic structure of monolayer FeSe is further analyzed by ARPES and large-bias tunneling spectra. We successfully identified two superconducting coherence peaks at  $V_i$  around 10 meV and  $V_o$  around 15-17 meV. Interestingly, by comparing the tunneling spectra at  $\alpha$  and  $\beta$  Fe, we find there are sublattice dichotomy effects. More precisely, the tunneling peak of  $\alpha$ -Fe at  $+V_i$  is larger than  $\beta$ -Fe while the coherence peak of  $\beta$ -Fe at  $-V_i$  is also larger than  $\alpha$ -Fe with a similar difference. We also observed a reversed effect at  $\pm V_o$ . We propose the  $\eta$ -pairing mechanism between  $k$  and  $-k + \mathbf{Q}$  is the key mechanism beyond conventional pairing considera-



tion.

*Acknowledgement* The work is supported by the National Key Research and Development Program of China (Grant No. 2022YFA1403100 and No. 2022YFA1403900), the National Natural Science Foundation of China (Grant No. 1888101, No. 12174428, No. 11920101005, No. 52388201 and No. 12074210), the Strategic Priority Research Program of the Chinese Academy of Sciences (Grant No. XDB28000000 and No. XDB33000000), the New Cornerstone Investigator Program, the Chinese Academy of Sciences Project for Young Scientists in Basic Research (2022YSBR-048), and the Basic and Applied Basic Research Major Programme of Guangdong Province, China (Grant No. 2021B0301030003) and Jihua Laboratory (Project No. X210141TL210).

*Contributions* C. D. and X. J. carried out the STM experiments; Q. H., W. Z. and L. Y. performed the ARPES experiments; J-F. J., L. W. and Q-K.X. designed and coordinated the experiments; Z-P.X, K.J. and J-P.H. perform the theoretical analysis. K. J., L. W., J-P. H and Q-K.X. wrote the manuscript with comments from all authors.

---

\* Cui Ding and Zhipeng Xu contributed equally to this work.

- [1] Qing-Yan Wang, Zhi Li, Wen-Hao Zhang, Zuo-Cheng Zhang, Jin-Song Zhang, Wei Li, Hao Ding, Yun-Bo Ou, Peng Deng, Kai Chang, *et al.*, “Interface-induced high-temperature superconductivity in single unit-cell fese films on sratio3,” *Chinese Physics Letters* **29**, 037402 (2012).
- [2] Wen-Hao Zhang, Yi Sun, Jin-Song Zhang, Fang-Sen Li, Ming-Hua Guo, Yan-Fei Zhao, Hui-Min Zhang, Jun-Ping Peng, Ying Xing, Hui-Chao Wang, *et al.*, “Direct observation of high-temperature superconductivity in one-unit-cell fese films,” *Chinese Physics Letters* **31**, 017401 (2014).
- [3] Zuocheng Zhang, Yi-Hua Wang, Qi Song, Chang Liu, Rui Peng, KA Moler, Donglai Feng, and Yayu Wang, “Onset of the meissner effect at 65 k in fese thin film grown on nb-doped sratio 3 substrate,” *Science bulletin* **60**, 1301–1304 (2015).
- [4] Lili Wang, Xucun Ma, and Qi-Kun Xue, “Interface high-temperature superconductivity,” *Superconductor Science and Technology* **29**, 123001 (2016).
- [5] Dennis Huang and Jennifer E. Hoffman, “Monolayer fese on sratio3,” *Annual Review of Condensed Matter Physics* **8**, 311–336 (2017).
- [6] Pengcheng Dai, “Antiferromagnetic order and spin dynamics in iron-based superconductors,” *Rev. Mod. Phys.* **87**, 855–896 (2015).
- [7] Johnpierre Paglione and Richard L. Greene, “High-temperature superconductivity in iron-based materials,” *Nature Physics* **6**, 645–658 (2010).
- [8] Defa Liu, Wenhao Zhang, Daixiang Mou, Junfeng He, Yun-Bo Ou, Qing-Yan Wang, Zhi Li, Lili Wang, Lin Zhao, Shaolong He, *et al.*, “Electronic origin of high-temperature superconductivity in single-layer fese superconductor,” *Nature Communications* **3**, 931 (2012).
- [9] Shaolong He, Junfeng He, Wenhao Zhang, Lin Zhao, Defa Liu, Xu Liu, Daixiang Mou, Yun-Bo Ou, Qing-Yan Wang, Zhi Li, Lili Wang, Yingying Peng, Yan Liu, Chaoyu Chen, Li Yu, Guodong Liu, Xiaoli Dong, Jun Zhang, Chuangtian Chen, Zuyan Xu, Xi Chen, Xucun Ma, Qikun Xue, and X. J. Zhou, “Phase diagram and electronic indication of high-temperature superconductivity at 65 k in single-layer fese films,” *Nature Materials* **12**, 605–610 (2013).
- [10] Shiyong Tan, Yan Zhang, Miao Xia, Zirong Ye, Fei Chen, Xin Xie, Rui Peng, Difei Xu, Qin Fan, Haichao Xu, Juan Jiang, Tong Zhang, Xinchun Lai, Tao Xiang, Jiangping Hu, Binping Xie, and Donglai Feng, “Interface-induced superconductivity and strain-dependent spin density waves in fese/sratio3 thin films,” *Nature Materials* **12**, 634–640 (2013).
- [11] J. J. Lee, F. T. Schmitt, R. G. Moore, S. Johnston, Y. T. Cui, W. Li, M. Yi, Z. K. Liu, M. Hashimoto, Y. Zhang, D. H. Lu, T. P. Devereaux, D. H. Lee, and Z. X. Shen, “Interfacial mode coupling as the origin of the enhancement of tc in fese films on sratio3,” *Nature* **515**, 245–248 (2014).
- [12] Chong Liu, Ryan P Day, Fengmiao Li, Ryan L Roemer, Sergey Zhdanovich, Sergey Gorovikov, Tor M Pedersen, Juan Jiang, Sangjae Lee, Michael Schneider, *et al.*, “High-order replica bands in monolayer fese/sratio3 revealed by polarization-dependent photoemission spectroscopy,” *Nature Communications* **12**, 4573 (2021).
- [13] Q. Fan, W. H. Zhang, X. Liu, Y. J. Yan, M. Q. Ren, R. Peng, H. C. Xu, B. P. Xie, J. P. Hu, T. Zhang, and D. L. Feng, “Plain s-wave superconductivity in single-layer fese on sratio3 probed by scanning tunnelling microscopy,” *Nature Physics* **11**, 946–952 (2015).
- [14] Dennis Huang, Can-Li Song, Tatiana A. Webb, Shiang Fang, Cui-Zu Chang, Jagadeesh S. Moodera, Efthimios Kaxiras, and Jennifer E. Hoffman, “Revealing the empty-state electronic structure of single-unit-cell FeSe/sratio<sub>3</sub>,” *Phys. Rev. Lett.* **115**, 017002 (2015).
- [15] Y Miyata, K Nakayama, K Sugawara, T Sato, and T Takahashi, “High-temperature superconductivity in potassium-coated multilayer fese thin films,” *Nature materials* **14**, 775–779 (2015).
- [16] Dung-Hai Lee, “What makes the tc of fese/sratio3 so high?” *Chinese Physics B* **24**, 117405 (2015).
- [17] Zi-Xiang Li, Fa Wang, Hong Yao, and Dung-Hai Lee, “What makes the tc of monolayer fese on sratio3 so high: a sign-problem-free quantum monte carlo study,” *Science Bulletin* **61**, 925–930 (2016).
- [18] Yi Gao, Yuting Wang, Tao Zhou, Huaixiang Huang, and Qiang-Hua Wang, “Possible pairing symmetry in the fese-based superconductors determined by quasiparticle interference,” *Phys. Rev. Lett.* **121**, 267005 (2018).
- [19] Yonghao Yuan, Xuemin Fan, Xintong Wang, Ke He, Yan Zhang, Qi-Kun Xue, and Wei Li, “Incommensurate smectic phase in close proximity to the high-t c superconductor fese/sratio3,” *Nature Communications* **12**, 2196 (2021).
- [20] Yu Xu, Hongtao Rong, Qingyan Wang, Dingsong Wu, Yong Hu, Yongqing Cai, Qiang Gao, Hongtao Yan, Cong Li, Chao-hui Yin, *et al.*, “Spectroscopic evidence of superconductivity pairing at 83 k in single-layer fese/sratio3 films,” *Nature Communications* **12**, 2840 (2021).
- [21] Fangsen Li, Qinghua Zhang, Chenjia Tang, Chong Liu, Jinan Shi, CaiNa Nie, Guanyu Zhou, Zheng Li, Wenhao Zhang, Can-Li Song, *et al.*, “Atomically resolved fese/sratio3 (001) interface structure by scanning transmission electron microscopy,” *2D Materials* **3**, 024002 (2016).
- [22] Yuki Fukaya, Guanyu Zhou, Fawei Zheng, Ping Zhang, Lili Wang, Qi-Kun Xue, and Shin-ichi Shamoto, “Asymmetrically optimized structure in a high-tc single unit-cell fese superconductor,” *Journal of Physics: Condensed Matter* **31**, 055701 (2018).
- [23] Fong-Chi Hsu, Jiu-Yong Luo, Kuo-Wei Yeh, Ta-Kun Chen, Tzu-Wen Huang, Phillip M Wu, Yong-Chi Lee, Yi-Lin Huang,

- Yan-Yi Chu, Der-Chung Yan, *et al.*, “Superconductivity in the pbo-type structure  $\alpha$ -fese,” Proceedings of the National Academy of Sciences **105**, 14262–14264 (2008).
- [24] Cui Ding, Zhongxu Wei, Wenfeng Dong, Hai Feng, Mingxia Shi, Lili Wang, Jin-Feng Jia, and Qi-Kun Xue, “Atomic-site dependent pairing gap in monolayer FeSe/SrTiO<sub>3</sub>(001)-(  $\sqrt{13} \times \sqrt{13}$ ),” arXiv preprint arXiv:2312.10723 (2023).
- [25] Jiangping Hu, “Iron-based superconductors as odd-parity superconductors,” *Phys. Rev. X* **3**, 031004 (2013).
- [26] Chen-Ning Yang, “ $\eta$  pairing and off-diagonal long-range order in a hubbard model,” *Phys. Rev. Lett.* **63**, 2144–2147 (1989).
- [27] Chen-Ning Yang and S.C. Zhang, “So4 symmetry in a hubbard model,” *Modern Physics Letters B* **04**, 759–766 (1990).
- [28] Pengfei Li, Kun Jiang, and Jiangping Hu, “Paramagnetic contribution in superconductors with different-mass cooper pairs,” (2023), arXiv:2311.16033.
- [29] Vladimir Cvetkovic and Oskar Vafek, “Space group symmetry, spin-orbit coupling, and the low-energy effective hamiltonian for iron-based superconductors,” *Phys. Rev. B* **88**, 134510 (2013).